Comparison of 2D and 3D neural induction methods for the generation of neural progenitor cells from human induced pluripotent stem cells

Chandrasekaran, Abinaya; Avci, Hasan X; Ochalek, Anna; Rösingh, Lone N; Molnár, Kinga; László, Lajos; Bellák, Tamás; Téglási, Annamária; Pesti, Krisztina; Mike, Arpad; Phanthong, Phetcharat; Bíró, Orsolya; Hall, Vanessa; Kitiyanant, Narisorn [**and 3 more**]

How to cite

CHANDRASEKARAN, Abinaya et al. Comparison of 2D and 3D neural induction methods for the generation of neural progenitor cells from human induced pluripotent stem cells. In: Stem Cell Research, 2017, vol. 25, p. 139–151. doi: 10.1016/j.scr.2017.10.010

This publication URL: https://archive-ouverte.unige.ch/unige:112338

Publication DOI: 10.1016/j.scr.2017.10.010

Stem Cell Research 25 (2017) 139–151

Contents lists available at ScienceDirect

Stem Cell Research

journal homepage: www.elsevier.com/locate/scr

Comparison of 2D and 3D neural induction methods for the generation of neural progenitor cells from human induced pluripotent stem cells

Abinaya Chandrasekaran [a,c], Hasan X. Avci [a,b], Anna Ochalek [a,c], Lone N. Rösingh [d], Kinga Molnár [e], Lajos László [e], Tamás Bellák [a,b], Annamária Téglási [a], Krisztina Pesti [f,g], Arpad Mike [f], Phetcharat Phanthong [a,h], Orsolya Bíró [i], Vanessa Hall [j], Narisorn Kitiyanant [h], Karl-Heinz Krause [d], Julianna Kobolák [a], András Dinnyés [a,c,*]

[a] BioTalentum Ltd, Gödöllő, Hungary
[b] Department of Anatomy, Embryology and Histology, Faculty of Medicine, University of Szeged, Szeged, Hungary
[c] Molecular Animal Biotechnology Lab, Szent István University, Gödöllő, Hungary
[d] Department of Pathology and Immunology, University of Geneva Medical School, Geneva, Switzerland
[e] Department of Anatomy, Cell and Developmental Biology, Eötvös Loránd University, Budapest, Hungary
[f] Opto-Neuropharmacology Group, MTA-ELTE NAP B, Budapest, Hungary
[g] János Szentágothai Doctoral School of Neurosciences, Semmelweis University, Budapest, Hungary
[h] Stem Cell Research Group, Institute of Molecular Biosciences, Mahidol University, Nakhon Pathom Bangkok, Thailand
[i] First Department of Obstetrics and Gynaecology, Semmelweis University, Budapest, Hungary
[j] Department of Veterinary and Animal Science, University of Copenhagen, Denmark

ARTICLE INFO

Article history:
Received 22 March 2017
Received in revised form 6 October 2017
Accepted 10 October 2017
Available online 14 October 2017

Keywords:
Neural induction
Neural progenitor cells
hiPSC
Electron microscopy
Patch clamp
2D-3D neural induction

ABSTRACT

Neural progenitor cells (NPCs) from human induced pluripotent stem cells (hiPSCs) are frequently induced using 3D culture methodologies however, it is unknown whether spheroid-based (3D) neural induction is actually superior to monolayer (2D) neural induction. Our aim was to compare the efficiency of 2D induction with 3D induction method in their ability to generate NPCs, and subsequently neurons and astrocytes. Neural differentiation was analysed at the protein level qualitatively by immunocytochemistry and quantitatively by flow cytometry for NPC (SOX1, PAX6, NESTIN), neuronal (MAP2, TUBB3), cortical layer (TBR1, CUX1) and glial markers (SOX9, GFAP, AQP4). Electron microscopy demonstrated that both methods resulted in morphologically similar neural rosettes. However, quantification of NPCs derived from 3D neural induction exhibited an increase in the number of PAX6/NESTIN double positive cells and the derived neurons exhibited longer neurites. In contrast, 2D neural induction resulted in more SOX1 positive cells. While 2D monolayer induction resulted in slightly less mature neurons, at an early stage of differentiation, the patch clamp analysis failed to reveal any significant differences between the electrophysiological properties between the two induction methods. In conclusion, 3D neural induction increases the yield of $PAX6^+/NESTIN^+$ cells and gives rise to neurons with longer neurites, which might be an advantage for the production of forebrain cortical neurons, highlighting the potential of 3D neural induction, independent of iPSCs' genetic background.

1. Introduction

The successful development of in vitro human models of disease is highly dependent on the availability of tissues and specific cell types from patients. These models can provide insights into disease phenotypes, pathomechanisms and help to reveal potential new targets for the development of new treatments (Hossini et al., 2015). Although primary cells isolated from patient tissue is the most physiologically relevant, this is often difficult to obtain, culture in vitro, and frequently has a limited life span (Yuan et al., 2013). Additionally, these biopsies are often taken from patients at the end-stage of the disease and suitable control tissues taken from healthy individuals might be inaccessible, due to ethical concerns and potential health risks (Hossini et al.,

Abbreviations: AD, Alzheimer's disease; AQP4, Aquaporin 4; ASD, Autism spectrum disorder; bFGF, Basic Fibroblast Growth Factor; CNS, Central Nervous System; D, Day; DAPI, 4',6-diamidino-2-phenylindole; DMSO, Dimethyl sulfoxide; EM, Expansion Medium; ESC, Embryonic Stem Cell; FBS, Foetal Bovine Serum; GFAP, Glial fibrillary acidic protein; hiPSC, human induced Pluripotent Stem Cell; ICC, Immunocytochemistry; IGF-1, Insulin-like Growth Factor-1; iPSC, induced Pluripotent Stem Cell; LGIC, Ligand-gated ion channel; NCC, Neural crest cell; NEP, Neural epithelial progenitor; NIM, Neural induction media; NMM, Neural maintenance media; NPC, Neural progenitor cell; PFA, Paraformaldehyde; PSC, Pluripotent Stem Cell; RT, Room Temperature; RT-PCR, Reverse transcription polymerase chain reaction; SCF, Stem Cell Factor.

* Corresponding author at: BioTalentum Ltd, Gödöllő, Hungary.
E-mail address: Manuscript.Dinnyes@biotalentum.hu (A. Dinnyés).

https://doi.org/10.1016/j.scr.2017.10.010

2015). Human induced pluripotent stem cells (hiPSCs) overcome many of these limitations (Takahashi and Yamanaka, 2006). These autologous cells can easily be derived from patients with known or unknown genetic mutations and have been produced from patients with sporadic Alzheimer's disease (AD) (Yang et al., 2016), Autism spectrum disorder (Nestor et al., 2016), Parkinson's disease (Holmqvist et al., 2016) and Amyotrophic lateral sclerosis (Bohl et al., 2016). In recent years, considerable progress has been made in understanding the mechanisms underlying the pathophysiology of certain diseases (Grskovic et al., 2011), which could serve as cell-based disease models for screening chemical libraries (Boissart et al., 2013).

Recent research suggests the environmental cues can fundamentally change the fate of a specific cell type (Tibbitt and Anseth, 2012). For example, stiffness of the material surrounding mesenchymal stem cells (MSCs) is sufficient to direct them into the neuronal lineage (Engler et al., 2006). Today, great progress has been achieved in this area in regards to comparison of the 2D and 3D microenvironment. Zhou and colleagues have directly established a link between the expression of PAX6 and astrocyte differentiation in 3D propagation protocols (Zhou et al., 2016). Other groups have also addressed the role of the matrix microenvironment (such as the architecture, type, composition) and shown that it is essential for differentiating stem cells into specific neural and glial lineages (Kothapalli and Kamm, 2013). Despite these findings, an extensive understanding of this dynamic environment is still limited.

Neural progenitor cells (NPCs) are self-renewing and have the capacity to differentiate into neurons as well as glia (Breunig et al., 2011). There are many established protocols for generating pluripotent stem cell (PSC)-derived cortical projection neurons from both mouse (Gaspard et al., 2009) and human cells (Shi et al., 2012a,b). However, efficient differentiation of these cells into specific neuronal subtypes remains challenging due to a large variation in outcomes following differentiation. This variation is likely due to the environmental niche, heterogeneity in starting cell populations, differences in culture media and altered handling of cells (Engler et al., 2006). The crucial step in generating NPCs is to efficiently induce PSCs into early neuroepithelial progenitors (NEP) (Chambers et al., 2009). Another prominent feature is the generation of neural "rosettes", which are morphologically identifiable structures containing neural progenitor cells, and which are believed to mimic the initial process of in vivo neural development (Wilson and Stice, 2006).

Over the years, NPCs derived from human PSCs have conventionally been induced using 3D aggregate systems, which are considered an efficient differentiation protocol of inducing PSCs into the neural lineage (Emdad et al., 2012). In addition, studies revealed that neural induction in 3D micro fibrous matrices also resulted in increased expression of NPC markers, as well as more mature neuron markers when compared to 2D neural induction (Liu et al., 2013). Despite these positive results, the 3D neural induction endures technical difficulties, such as, low efficiencies of cells forming 3D spheres, or difficulties in controlling the sphere's size and shape. In order to overcome these technical challenges, 2D neural induction was implemented to generate NPCs at a higher efficiency (Yan et al., 2013). Although Muratore et al. compared the commonly employed methods for neuronal differentiation from iPSCs, no analysis of the initial neural induction changes was performed (Muratore et al., 2014). In addition, no publication has directly compared 3D neural induction (sphere) versus 2D neural induction (adherent, monolayer), and which specifically analyses differences between cell numbers, gene expression profiles, proliferation rates, differentiation potential, cell fate, or even functionality.

In the current study, we provide specific comparisons of these two systems following differentiation from five different hiPSC lines with different genetic backgrounds (healthy controls and patient-derived cell lines). We identified that neural rosettes could be generated from both induction methods, which later differentiated into mature cortical neurons. However, we found that the 3D neural induction method yielded a higher number of NPCs and neurons with longer neurites. Electrophysiological studies did not reveal significant differences between the two different methods or cell lines, suggesting no profound changes in function was observed.

2. Materials and methods

The chemicals were purchased from Sigma-Aldrich (St Louis, MO, USA) and the cell culture reagents and culture plates were purchased from Thermo Fisher Scientific (Waltham, MA, USA), unless specified otherwise.

2.1. Cell lines and their culture

In this study, five different genetic background hiPSC lines were used. Three cell lines were derived from AD patients, which have been established and characterized previously; DL-1 (Nemes et al., 2016); DL-2 (Chandrasekaran et al., 2016) and DL-3 (Ochalek et al., 2016); and two hiPSC lines were healthy individual-derived iPSC lines, CTL-2 and CTL-3 (Zhou et al., 2016) which were established, characterized and maintained identically to the AD iPSC lines. The hiPSC lines were maintained on Matrigel (BD Matrigel; Stem Cell Technologies) in mTESR1 (Stem Cell Technologies) culture media. The media was changed daily and the cells were passaged every 5–7 days using Gentle Cell Dissociation Reagent (Stem Cell Technologies), according to the manufacturer's instructions.

2.2. Monolayer based (2D) neural induction

Dual inhibition of the SMAD signaling pathway was chosen as the 2D neural induction method (Chambers et al., 2009; Shi et al., 2012a,b) (See details in Supplementary Fig. 1). Differentiation was induced by 10 μM SB431542 and 500 ng/mL Noggin (R&D) in neural induction medium (NIM; see details in Supplementary methods) for 10 days. Neural rosettes were manually picked and re-plated onto POL/L plates. Up to passage 4, rosette-like structures were plated *en bloc* on POL/L plates, without dissociation. From passage 4, the cells were seeded as single cells (min 50.000 cells/cm^2) using Accutase and NPCs were further cultured and expanded in neural maintenance medium (NMM). For further details see Supplementary methods.

2.3. Sphere based 3D neural induction

To generate 3D spheres, the iPSCs cells were dissociated using Gentle Cell Dissociation Reagent and were plated on non-adherent plates to enhance the cell aggregation. At the time of plating (Day 1) the cells were seeded as clumps with an average size of 80–100 cells/clump (approximately 1.0×10^7 cells/mL) in NIM. The NIM media, containing Noggin (500 ng/mL) and SB431542 (10 μM), was changed daily until Day 9. On Day 8, the floating spheres were moved onto POL/L-coated plates for attachment and outgrowth. To detach the formed neural rosettes, they were gently flushed from the plate surface by treating with Accutase for 3 min and were plated as small clumps in POL/L coated dish in NMM media, supplemented with 10 ng/mL of bFGF and 10 ng/mL of EGF. Upon reaching confluence, NPCs were passaged and plated onto new POL/L plates, expanded and analysed in a way similar to the 2D neuronal induction method (Supplementary Fig. 1). For further details see Supplementary methods.

2.4. Fluorescence activated cell sorting (FACS)

NPCs were collected using 0.5% trypsin to obtain a single cell suspension which was then fixed in 4% paraformaldehyde (PFA) for 20 min at room temperature (RT). After fixation, the cells were permeabilized with 0.2% Triton X-100 (5 min at RT), followed by blocking with 1% BSA (15 min, RT). The cells were then incubated with the corresponding

antibodies for 1 h at RT. For unconjugated primary antibodies the isotype specific secondary antibodies were used accordingly (for details see Supplementary methods and tables: Suppl. Table 1). Samples were analysed using 'Flow Cytometer Cytomics FC 500′ (Beckman Coulter). Data was analysed using the FlowJo software (version 7.6.5; FlowJo, LLC).

2.5. Immunocytochemistry

Cell cultures were fixed in 4% PFA (20 min, RT), washed 3 times with PBS and permeabilized (0.2% triton X-100 in PBS; 20 min). After blocking for 40 min (at RT in 3% BSA) the cells were incubated with primary antibodies (see details and dilutions in Supplementary methods and tables: Suppl. Table 1) overnight at 4 °C. On the following day, the isotype specific secondary antibodies (for details see Supplementary methods and tables: Suppl. Table 1) were applied (1 h at RT). Samples were mounted with Vectashield mounting medium containing DAPI (1.5 μg/mL; Vector Laboratories) to label the nuclei of the cells. Samples were visualized on a fluorescence microscope equipped with a 3D imaging module (AxioImager system with ApoTome, Carl Zeiss MicroImaging GmbH) controlled by AxioVision 4.8.1 software.

Fixed 3D neural induction derived spheres were embedded in Shandon Cryomatrix gel (Thermo Fischer Scientific) according to the manufacturer's instructions, and 10 μm parallel sections were cryo-sectioned (Leica CM 1850 Cryostat, Leica GmbH) and stored at −20 °C freezer until use. Immunostainings was performed as above and sections were analysed using FluoView FV10i confocal laser scanning microscope (Olympus Ltd., Tokyo, Japan).

2.6. Electron microscopy

Evaluation of the ultrastructural characteristics of the 2D and 3D neural induction derived NPCs was performed in one control line (CTL-2) and one disease line (DL-2). The 2D neuroepithelial sheets were grown on POL/L coated coverslips (at Day 8 of the induction phase) and the 3D neural induction-derived free-floating spheres (at Day 8 of the induction phase) were fixed (3.2% PFA, 0.2% glutaraldehyde, 1% sucrose, 40 mM $CaCl_2$ in 0.1 M cacodylate buffer) for 24 h (4 °C). Samples were rinsed for 2 days in cacodylate buffer, then postfixed in 1% ferrocyanide-reduced osmium tetroxide (White et al., 1979) for 1 h (RT). The samples were then treated with aqueous 1% uranyl-acetate for 30 min and embedded in Spurr low viscosity epoxy resin medium (Sigma), according to the manufacturer's instructions, and cured for 24 h at 80 °C. Ultrathin sections were stained with 2.5% aqueous uranyl acetate for 10 min an Reynolds's lead citrate for 2 min and examined in a JEOL JEM 1011 transmission electron microscope, operating at 60 kV. Photographs were taken using Olympus Morada 11 megapixel camera and iTEM software (Olympus).

2.7. Quantitative reverse transcription PCR (qRT-PCR)

Total RNA was isolated from NPCs and differentiated neurons using the RNeasy mini extraction kit (Qiagen) according to the manufacturer's protocol. A total of 500 ng of RNA was transcribed using Superscript III VILO cDNA synthesis kit (Thermo Fisher Scientific). The PCR conditions were subjected to 94 °C, 3 min, initial denaturation; followed by 40 cycles of 95 °C, 5 s, denaturation; 60 °C 15 s, annealing and 72 °C 30 s, elongation. The amplification reactions were carried out in a total volume of 15 μL using SYBR Green Master Mix (Thermo Fisher Scientific). Human *GAPDH* and Beta-2-Microglobulin (*B2M*) were used as reference genes. The data was analysed using REST software (2009 V2.0.13) and the statistics were analysed using Graph Pad prism 5. Values are expressed as ± SEM as indicated by Fig. legend text. Statistical significance was tested with an unpaired student *t*-test (two tailed) for evaluating differences between two groups; and by a one way ANOVA with a Tukey's post-test for testing differences between two or more groups. Statistically significant differences were determined when p values were <0.05 ($p < 0.05$). Oligonucleotide primers used in this study are listed in Supplementary methods and tables: Suppl. Table 2. In the current study, iPSC-derived NPCs (from 2D & 3D) were differentiated towards neurons for 5 weeks (35 days) for the qRT-PCR analysis.

2.8. Neurite length measurements

Human iPSC-derived neurons derived from both 2D and 3D neural inductions (at Day 25) were dissociated with accutase for 3 min and replated on POL/L (0.002%/1 μg/cm^2) coated coverslips in 24-well plates for neurite length analysis (10.000 cells/cm^2). The plated cells were cultured for a further 5 days and thereafter fixed with 4% PFA, immunostained and analysed. Neurite length was assessed using neurite tracer software of ImageJ. The analysis was carried out blinded by an independent investigator. For details see Supplementary methods.

2.9. Electrophysiological recordings

Standard patch clamp electrophysiology experiments were performed on eight week old terminally differentiated neuron cultures. Whole cell recordings were carried out using an Axopatch 200 B amplifier and the pClamp software (Molecular Devices, Sunnyvale, CA). For further details see Supplementary methods.

2.10. Statistical analysis

For all experiments, data are represented as Mean ± SEM from 3 independent biological replicates. Statistical analysis was determined using a two-tailed Student's *t*-test (for gene expression, FACS) or by one way ANOVA with a Tukey's post-test for differences of mean between each group of data with parametric distribution. Significant comparison were labelled in figures as ($^*p < 0.05$, $^{**}p < 0.01$).

3. Results

3.1. Dual SMAD inhibition efficiently induces neural rosette formation of iPSCs in both 2D and 3D cultures

We compared two neural induction methods to generate neural progenitor cells (NPCs); (2D neural induction and 3D neural induction). In the 2D neural induction method a neuroepithelial cell sheet formed, where the majority of the cells organized in 'rosettes' expressed SOX1, (a marker of early NEP cells) NESTIN and PAX6 (Fig. 1) after 10 days of culture. The bright field images illustrated in Supplementary Figs. 1 and 2 exemplify the morphological changes over the course of the induction.

In the case of the sphere-based 3D neural induction, aggregates began to emerge around Day 4 following the neural induction. Following the sphere formation (between Day 4–8), the spherical aggregates showed similarities across the five different cell lines by gross morphological analysis (Supplementary Fig. 2). We did not observe morphological differences in the efficiency of spheroid formation among the different hiPSC lines (data not shown). As shown in Fig. 1, the majority of the cells co-expressed NESTIN and PAX6, and were positive for SOX1. In both induction methods several cells were positive for Ki-67 a marker or dividing cells (Fig. 1).

Neural rosettes were observed in induction methods, which were observed by phase contrast microscopy (Supplementary Fig. 2), confocal microscopy (Fig. 1) and even electron microscopy (Fig. 2). In semithin TEM sections, we observed several neural rosettes in various sizes and shape (e.g. the number of cells forming the rosette), which we believe is connected to the age of the rosettes (dependent on which day during the induction they started to form). On the basis of their regular pattern we called the area of the rosettes as zone I (Fig. 2A–D). Central cavities contained cell debris or rarely intact cells

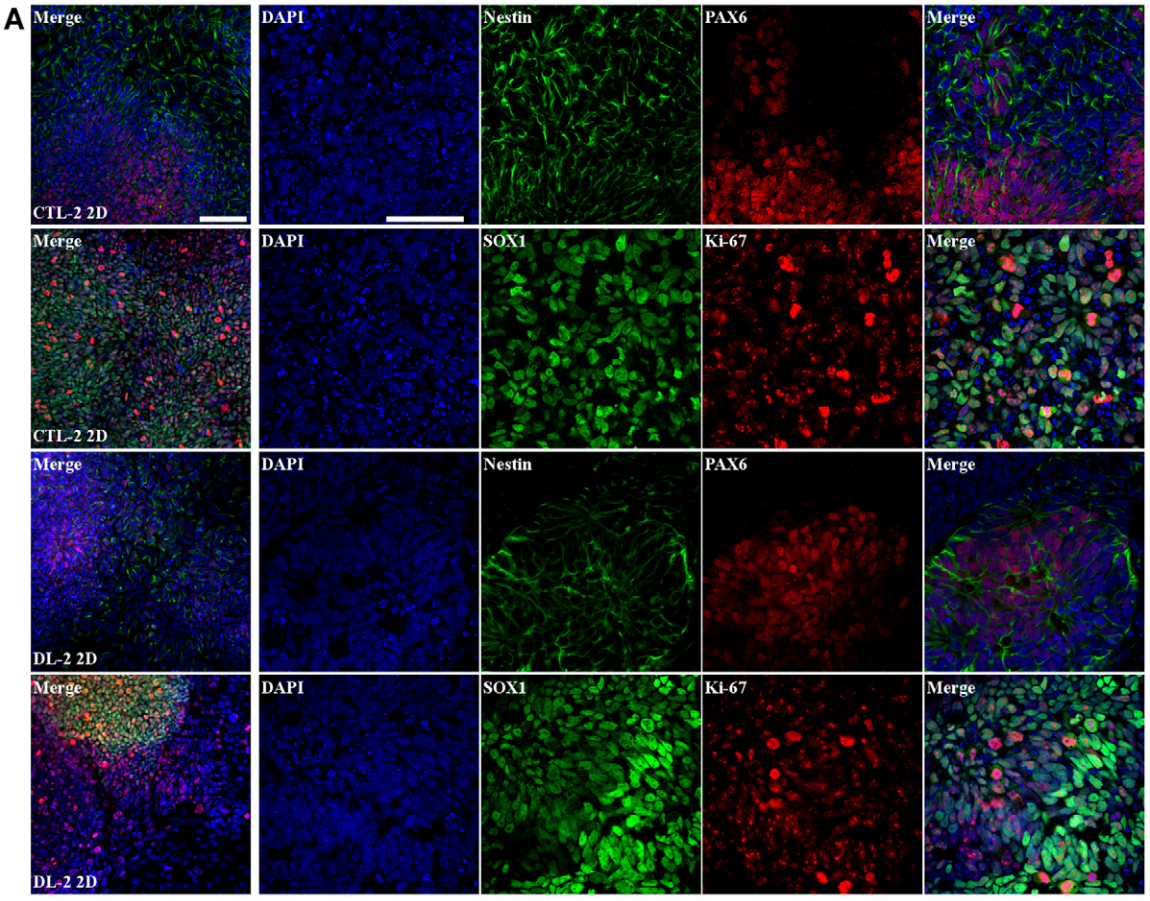
A
Merge
DAPI
Nestin
PAX6
Merge
CTL-2 2D
Merge
DAPI
SOX1
Ki-67
Merge
CTL-2 2D
Merge
DAPI
Nestin
PAX6
Merge
DL-2 2D
Merge
DAPI
SOX1
Ki-67
Merge
DL-2 2D

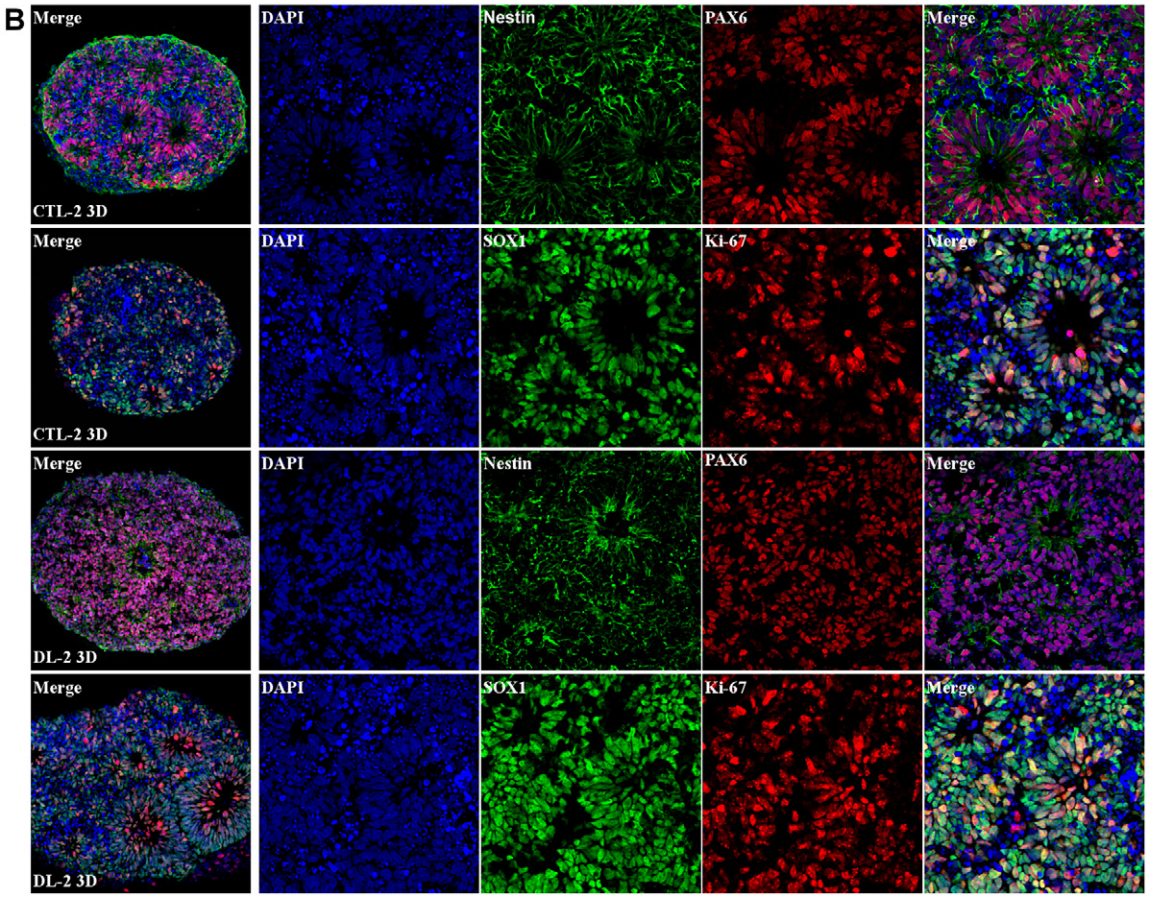
B
Merge
DAPI
Nestin
PAX6
Merge
CTL-2 3D
Merge
DAPI
SOX1
Ki-67
Merge
CTL-2 3D
Merge
DAPI
Nestin
PAX6
Merge
DL-2 3D
Merge
DAPI
SOX1
Ki-67
Merge
DL-2 3D

(Fig. 2E–H). Long, radially ordered cells surrounding the central cavity showed ultrastructural features typical of radial glial cells, including cell coupling *zonula adherens* and tight junctions, deposits of glycogen storage granules and cilia (Kriegstein and Alvarez-Buylla, 2009) (Fig. 2I–L). A network of smaller, multipolar cells among the rosettes formed a second zone (zone II) (Fig. 2A–D). The cells in zone II contained smaller glycogen deposits and lipid droplets (Fig. 2M). We observed mitotic cells both in the vicinity of the central cavities (Fig. 2H) and further away from the centre of the rosettes (Fig. 2N–P).

In summary, early events such as neuroepithelial commitment and neural rosette formation of the cells were observed, structural changes were clearly distinguished and specific neuronal markers were already identifiable with ICC without detecting significant differences between the two induction methods or the different genetic background cell lines.

3.2. A higher amount of PAX6$^+$/NESTIN$^+$ neural progenitor cells are generated using 3D neural induction

Following 4 passages of the rosettes, the morphology of NPCs was assessed by phase contrast imaging and for the expression of varying neural lineage markers by ICC. Continual passaging resulted in NPCs proliferating on a monolayer surface; however cells from both methods continued to form rosette-like structures during the cell passaging (Fig. 3A).

Next, we quantified the NPC populations. FACS analysis showed that the average proportion of NESTIN and PAX6 double positive cells in 2D was 83% ± 1.73 (mean ± SEM) and in 3D was 93.34% ± 1.55 (mean ± SEM; $p < 0.05$; Fig. 3B and C; Supplementary methods and tables: Supplementary Table 3). When tested for statistical differences between both methods, there was an average of 10% ± 0.148 (mean ± SEM) difference between the two induction methods with a significant increase in 3D cultures ($p < 0.05$; Supplementary methods and tables: Supplementary Table 3). Hereby indicating 3D was superior to 2D. Of particular interest was the presence of two PAX6 positive cell populations with both methods. One population was strongly positive for PAX6, whilst the other population expressed PAX6 at lower levels (Fig. 3A). This is in accordance with our previous study where we observed similar differences in NPCs derived from hiPSCs (Zhou et al., 2016a). Taken together, the results indicate that the proportion of PAX6$^+$ and NESTIN$^+$ NPCs was significantly higher when using the 3D neural induction method.

3.3. The 2D neural induction increases the expression of SOX1

In order to study the neural fate of the generated NPCs, we investigated the expression of two important markers, SOX1 which marks the NPCs and the neural crest marker, SOX9. In both induction methods, the passage five (p5) NPCs maintained their expression of SOX1, whilst a small population was positive for SOX9 (Fig. 4A). Recent studies have suggested that the transcription factor SOX9 is highly enriched in astrocytes (Sun et al., 2017; Farmer et al., 2016; Zhang et al., 2016a,b). In order to assess the expression, we quantified the SOX1 and SOX9 population using FACS (Fig. 4B). The proportion of SOX1$^+$ cells was 86.1% ± 2.02 (mean ± SEM) in the 2D neural induction, while in the 3D neural induction it was 76.4% ± 1.8 (mean ± SEM). Subsequently, we found that the neural crest population within the generated NPCs (i.e. the proportion of SOX9$^+$ cells) was 8.51% ± 0.838 (mean ± SEM) in 2D cultures and 12.3% ± 0.961 (mean ± SEM) in the 3D cultures. (See detailed data in Supplementary Table 3; $p < 0.05$; Fig. 4B). Based on quantitative FACS data, we can conclude that the 2D neural induction method generated more SOX1 positive neural progenitor cells in all of our examined cell lines.

3.4. Terminal differentiation of the NPCs revealed similar neuronal fate

We then evaluated neuronal fate by performing ICC and quantitative RT-PCR using varying neuronal markers. The ICC analysis showed that the majority of cells derived from the NPCs' from the two induction methods were positive for tubulin, beta 3 class III (TUBB3), and microtubule-associated protein 2 (MAP2). These neurons also contained long neurites (Fig. 5A). As shown in Fig. 5A, all the differentiated neurons exhibited fasciculation bundles. In order to quantify and compare the expression level of several markers and their gene expression profile, qRT-PCR was performed on terminally differentiated neurons. As expected, a steady increase in the *TUBB3* (2D = up to 6-folds increase and 3D = up to 7-folds increase) and *MAP2* expression (2D = up to 11-folds increase and 3D = up to 12-folds increase) was observed (Fig. 5B). Our qRT-PCR data showed that 4 out of 5 lines had a very modest increase in *TUBB3* and *MAP2* expression level in the 3D neural induction method at the mRNA level.

We then examined the expression of the cortical layer markers *CUX1* (*cut-like homeobox 1*; expressed in IV-II layer of late born/upper layer cortical neuron) (Nieto et al., 2004) and *TBR1* (*T-box*, *brain, 1*; labels the cortical neurons and are widely expressed in layer IV) (Hadjivassiliou et al., 2010) (Fig. 6A). As shown in Fig. 6B, a slightly higher amount of TBR1 positive cells [ranging from 2D: 9.34% up to 22.39% (SEM ± 0.93 and SEM ± 2.20), while in 3D: 7.03% up to 22.2% (SEM ± 0.96 and SEM ± 4.95), respectively] were found in the NPCs derived from both neural inductions as compared to CUX1 [2D = 10.56% up to 14.23% (SEM ± 1.69 and SEM ± 1.15), while in 3D = 7.16% up to 18.98% (SEM ± 0.86and SEM ± 5.60), respectively] (Supplementary methods and tables: Suppl. Table 3; $p < 0.05$).

Subsequently, we also evaluated the expression of glial subtype markers glial fibrillary acidic protein (GFAP) and aquaporin-4 (AQP4) (Roybon et al., 2013) at a late stage in differentiation (week 11; Fig. 6C). Based on our results, a large variation in the proportion of GFAP positive cells could be determined across both induction methods [2D: 3.12% up to 45.29% (SEM ± 0.12 and SEM ± 1.69), 3D: 5.27% up to 48.11% (SEM ± 0.75 and SEM ± 11.41, respectively]. In the case of AQP4, a large variation was also detected, but was generally lower than GFAP [2D: 1% up to 36.43% (SEM ± 0.23 and SEM ± 3.0), 3D: 6.60% up to 32.20% (SEM ± 1.90 and SEM ± 4.74, respectively] (Supplementary methods and tables: Suppl. Table 3; $p < 0.05$; Fig. 6D). This result indicates that both neural induction methods promote the differentiation of cortical neurons, as well as glia and potentially radial glia, which also express GFAP. To conclude, cell line differences were relatively high and modest differences could be determined in neuronal fate when comparing the 2D and 3D neural induction methods; which needs to be clarified in future studies.

3.5. Neurite outgrowth showed significant difference among the two induction methods

Axonal growth and branching are essential for the formation of the nervous system (Jiang and Rao, 2005). The neurite length of neurons derived by both induction methods was investigated by comparing the neurite outgrowth after five days of terminal differentiation. At the time of plating the pre-differentiated neurons (Day 25) appeared spherical in shape with no apparent neurite outgrowth. About 24 h post-plating, thin neurites began to emerge from the cell bodies of the cells. Five

Fig. 1. Immunocytochemical characterisation of 2D and 3D neural induction derived neuronal rosettes from CTL-2 and DL-2 cultures. Neuronal progenitor cells forming neuronal rosette structures showed PAX6 (red) and NESTIN (green) and SOX1 (green) positivity. Dividing cells showed Ki-67 (red) expression (A) Representative confocal microscopic images of immunostained 2D neuroepithelial sheets grown on POL/L treated coverslips (B) Representative confocal microscopic images of 3D sphere and its cryosections. By ICC, structural differences were not observed. Nuclei were counterstained with DAPI (blue). *Left hand-side line*: Images recorded at 20× magnification and thereafter images recorded at 60× magnifications. Scale bar: 100 μm.

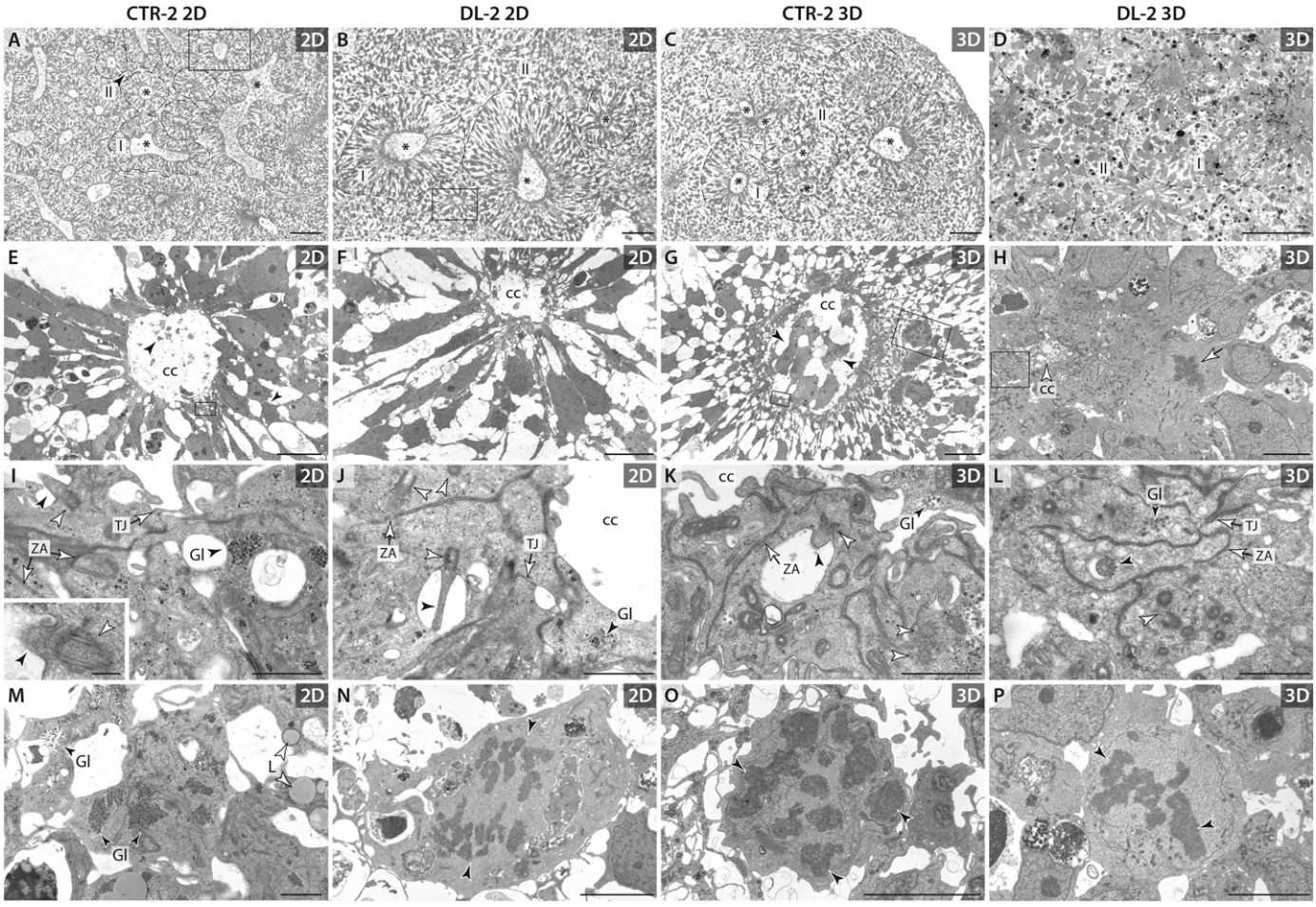

Fig. 2. Ultrastructural characterisation of CTL-2 and DL-2 cultures derived with 2D and 3D method. (A–D) Semithin sections represent neural rosettes with central cavities (*) surrounded by radially oriented cells (zone I). Cells among the rosettes form zone II. (E–H) Morphology of the rosettes on ultrathin sections at low magnification. The central cavities (cc) contain cell debris (panel E, black arrowheads) or intact cells (panel G, black arrowheads) and bordered by processes of narrow, radially oriented cells. White arrow shows a mitotic radial glial cell in panel H. (Panel E and F are magnified areas of panel A and B, respectively.) (I–L). Surface of the central cavities: cell coupling structures, i.e. tight junctions (TJ) and *zonula adherens* (ZA), cilia (black arrowheads), basal bodies (white arrowheads) and glycogen deposits (Gl) can be seen in the cell processes limiting the central cavity (cc). Inset I: basal body (white arrowhead) and cilium (black arrowhead) in longitudinal section. (Panel I and K are magnified areas of panel E and G, respectively.) (M) Cells further away the central cavity contain glycogen deposits (Gl) and lipid droplets (L). (N–P) Mitotic cells with condensed chromatin (black arrowheads) (scale bars: A–D: 50 μm, E–G: 10 μm, H, N-P: 5 μm; I–M: 1 μm, E inset: 100 nm).

days later, by the end of the differentiation period (at Day 30), many cells possessed between one and three neurites. Fig. 6E describes the way of analysis was performed. Analysis of neurite length revealed the 3D neural induction-derived neurons had longer neurites, ranging from 236.82 μm ± 12.705 up to 461.16 μm ± 25.21 (mean ± SEM), while in the 2D induction method, neurites were from 213.35 μm ± 13.36 up to 367.20 μm ± 26.52 (mean ± SEM). Cell line differences were also relatively high (Fig. 6F; Supplementary methods and tables: Suppl. Table 3; $p < 0.05$) and a remarkable and significant difference was observed within the differentiated neurites, suggesting the 3D method was more superior for neurite elongation.

3.6. Electrophysiology analysis

Functional analyses were deemed essential to verify the observation of longer neurite outgrowth in 3D neural-induced neurons. Therefore, eight week old neural cultures were analysed with patch clamp to determine if spontaneous activation and electrophysiological properties were different in neurons produced from both culture methods. Sodium and potassium channels were present in almost all cells analysed (40 out of 42 studied cells). There was no significant difference in the sodium and potassium current amplitudes between the two induction methods. Peak amplitude of sodium currents was 1.97 ± 0.36 nA (range: 0.3 to 2.8 nA) for the 2D cultures ($n = 7$), and 2.26 ± 0.36 nA (range: 0.1 to 8.2 nA) for the 3D cultures ($n = 35$). Fig. 7A and B shows examples for families of sodium currents evoked by the activation and the inactivation protocols, respectively. Examples of sodium currents from both induction methods are shown in Fig. 7C.

There was no significant difference between 2D and 3D neural induction-derived cultures in their spontaneous synaptic activity (observed in 4 out of 42 studied cells; an example is shown in Fig. 7D), or in their LGIC-mediated currents. The presence of AMPA receptors was shown by currents evoked by kainate, which was observed in 13 out of 19 tested cells. Fourteen cells out of 21 responded to GABA (1333 ± 392 pA), and 12 out of 17 responded to choline + PNU 120596 (749 ± 219 pA). Examples of LGIC-mediated currents are shown in Fig. 7E. In conclusion, spontaneous and evoked synaptic activity was detected in both types of cultures. There were no significant differences observed for the examined parameters which would be in correlation with the induction method. Overall, both methods were suitable to generate mature, synaptically active neurons following terminal differentiation.

4. Discussion

In our study, we performed a direct comparison of 2D neural induction and 3D neural induction methods to assess which of these might be more efficient in the production of cortical neurons.

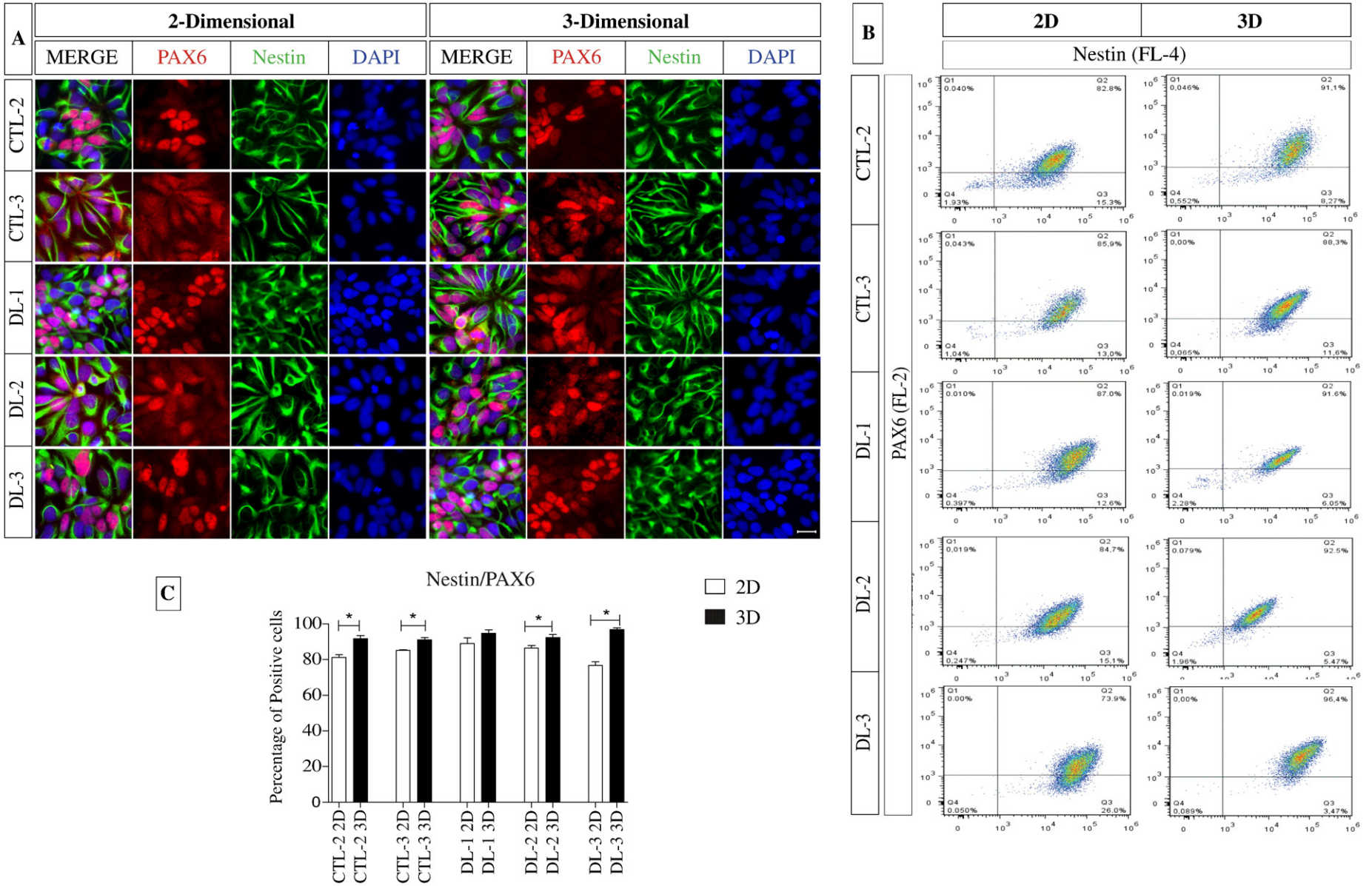

Fig. 3. Comparison of hiPSC derived NPC populations generated with 2D or 3D neural induction methods. (A) Immunocytochemical analysis of NPCs after induction. Neural progenitor markers, PAX6 (in red) and NESTIN (in green). Nuclei are counterstained with DAPI (in blue) Scale bar: 40 μm (B) Flow cytometer dot plots demonstrate PAX6 and NESTIN expression in a quantitative manner. The proportion of $PAX6^{+}$ and $NESTIN^{+}$ NPCs was significantly higher when the 3D neural induction method was applied, independent from the genetic background of the cell lines used (see details in Supplementary Table 1). From the dot plot Q1: $PAX6^{+}$ cells; Q2: $PAX6^{+}$ and $NESTIN^{+}$ cells; Q3: $NESTIN^{+}$ cells; Q4: $PAX6^{-}$ and $NESTIN^{-}$ cells. (C) Data analysis of dot plots into bar graphs, the bar graph illustrates the percentage of NESTIN and PAX6 positive cells; Test for significant difference ($^{*}p < 0.05$) using Student's *t*-test. The bars represent the mean ± SEM of 3 independent cultures set.

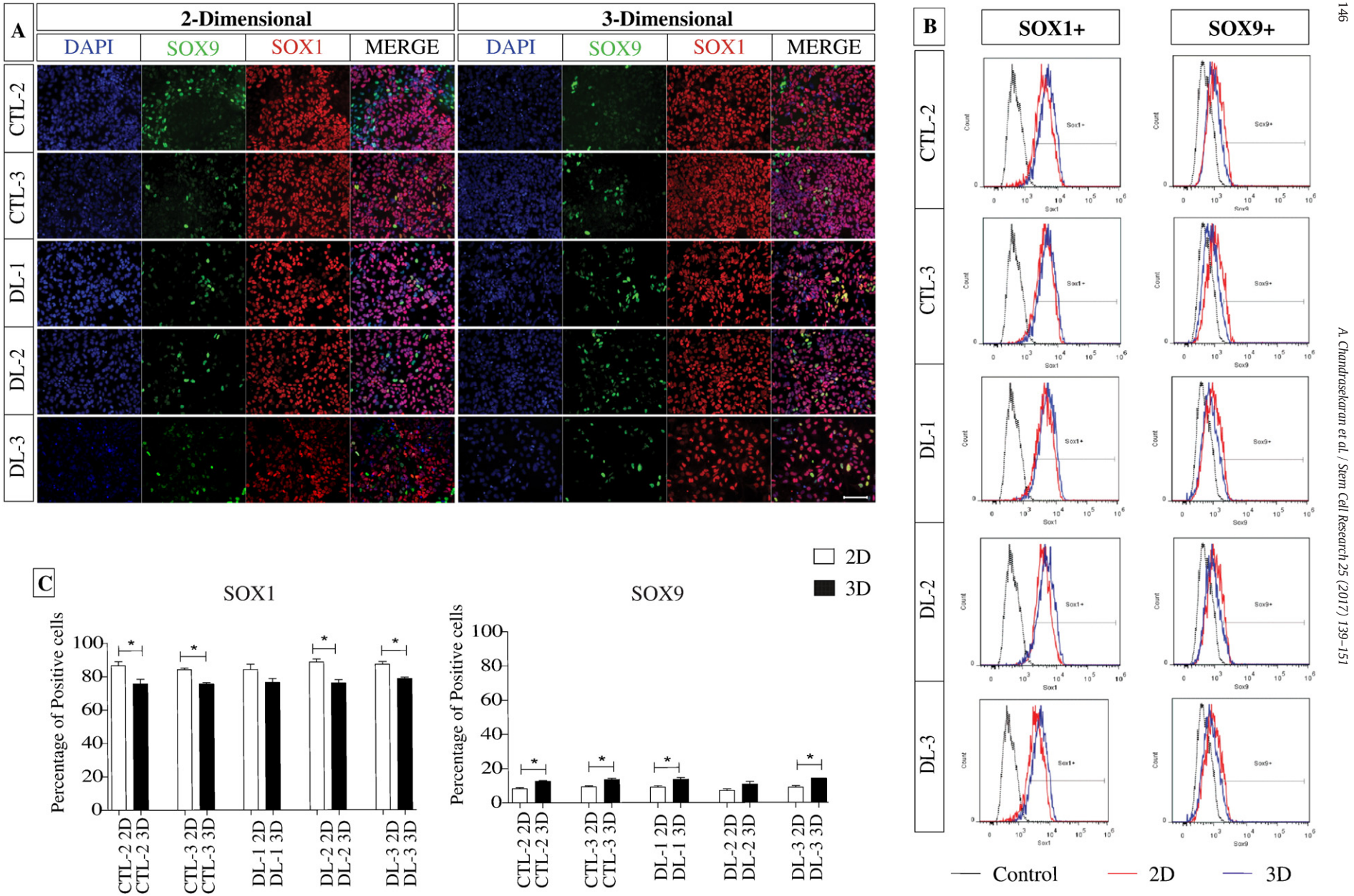

Fig. 4. Characterisation of neural progenitor cells derived with 2D and 3D neural induction methods. (A) Immunocytochemical analysis of SOX1 (in red) and SOX9 (in green) populations in 2D and 3D neural progenitor cells. Nuclei are counterstained with DAPI (in blue). Scale bar = 100 μm (B). Quantification of SOX1 and SOX9 expression with flow cytometry. Specific gating was applied to quantify the SOX1 and SOX9 expression populations. The histogram demonstrated that SOX1 and SOX9 expression in 2D and 3D NPCs was more homogeneous (C) Data analysis of FACS data into bar graphs. The bar graph illustrates the percentage of SOX1 and SOX9 positive cells; Test for significant difference (*$p < 0.05$) using Student's *t*-test. The bars represent the mean ± SEM of 3 independent cultures set.

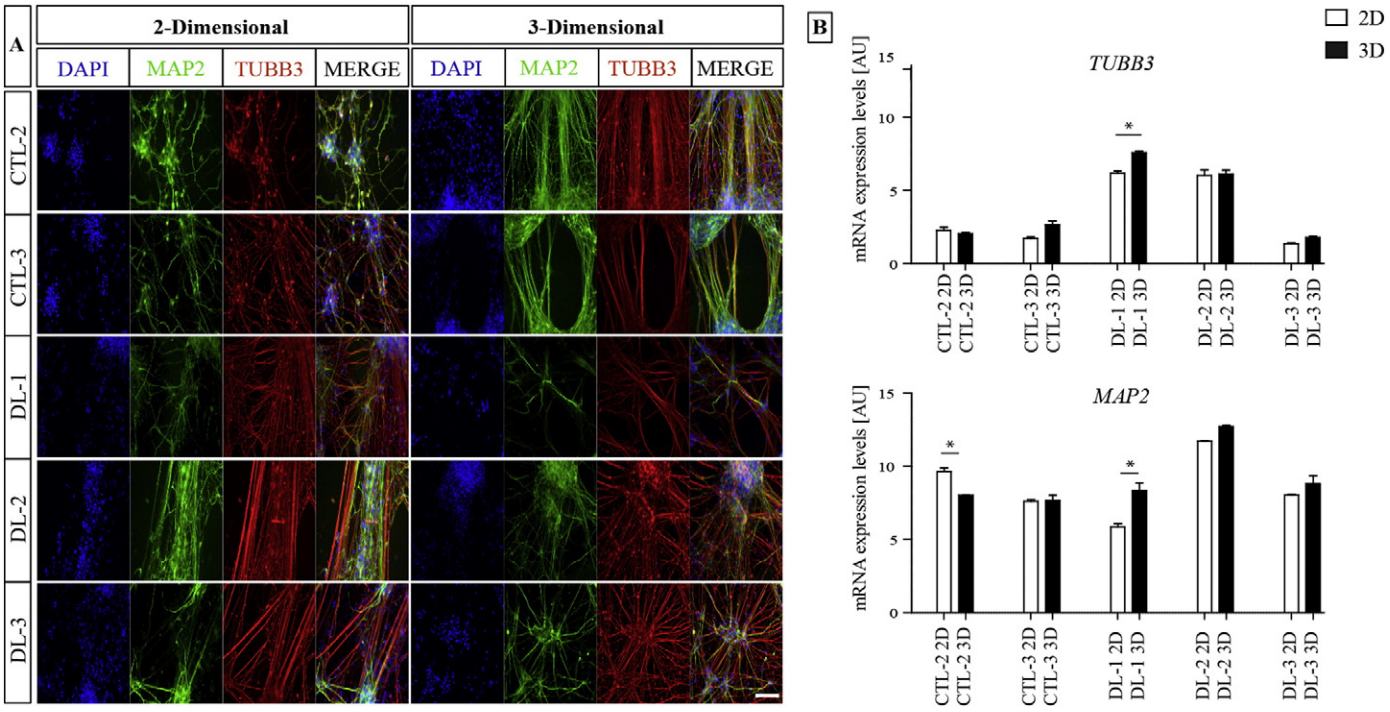

Fig. 5. Terminal differentiation of NPCs after 35 days revealed cortical neurons. (A) Representative immunocytochemical analysis shows MAP2 (in green) and TUBB3 (in red) in neurons differentiated from both induction methods. Nuclei are counterstained with DAPI (in blue). Scale bar = 100 μm (B) qRT-PCR analysis plots reveals the expression profile of terminally differentiated neurons from 2D NPCs and 3D NPCs. The expression value was normalized to *GAPDH* and *B2M*. Subsequently, the expression values were calculated as relative amount of mRNA versus expression values of differentiated cells. Test for significant difference were analysed using student *t*-test ($p < 0.05$).

The first successful induction of neurons from human PSCs was published by Zhang et al. in 2001 (Zhang et al., 2001). The efficiency of neural differentiation was enhanced by modulating pathways dependent on SMAD factors either alone, or by dual inhibition. Yao et al. reported the induction of neural differentiation of hESCs under culture conditions using the BMP inhibitor, Noggin. Addition of Noggin suppresses the induction of endodermal and mesodermal cell fates in suspension culture (Yao et al., 2006) while a small molecule SB431542, a selective inhibitor of the TGFβ pathway, inhibits SMAD signaling by modulating phosphorylation of ALK4, ALK5 and ALK7 receptors (Chambers et al., 2009; Wattanapanitch et al., 2014). Thus, this synergic inhibition of these two factors (BMP and TGFβ) alters the cellular fate of PSCs and directs them into the neural lineage (Chambers et al., 2009).

Using Zhang's method of induction, important comparisons have been made between the rosette stage and human embryo development stage (indicating the neural tube formation vs. the third week of gestation) (Pankratz et al., 2007). During neural induction, human PSC undergo morphogenetic events to form columnar epithelial cells termed "neural rosettes" (Perrier et al., 2004). These structures are capable of differentiating into various region-specific cells (neuronal and glial). Our findings clearly demonstrate that the neural rosettes produced by the synergistic inhibition of dual SMAD induction (BMP and TGF-β) exhibits similar neural rosette formation when both methods were used. Thus, the formation of neural rosette in vitro recapitulates the neural tube formation in vivo (Muguruma and Sasai, 2012). Following 10 days of neural induction, no morphological or qualitative differences in the ICC could be observed in the formed rosettes, suggesting a uniform expression of NPC markers in the NEP phase (such as SOX1, PAX6 and NESTIN) by both induction methods (2D and 3D).

Strikingly, our FACS analysis data showed a significant increase of PAX6/NESTIN double positive cells in the 3D neural induction method when NPCs were isolated from the rosettes. This observation is also in agreement with previously described findings by Zhou and colleagues (Zhou et al., 2016). This indicates that the 3D neural induction method results in more forebrain neurons (Mariani et al., 2012; Molyneaux et al., 2007).

PAX6 is a neuroectodermal marker (Onorati et al., 2014) in the differentiating human CNS and is expressed in the dorsal forebrain, including a region that gives rise to the cortex and functions in patterning the brain (Osumi, 2001). Study by Suter et al., suggested that overexpression of PAX6 in noncommitted cells favour neural lineage commitment by differentiation into radial glia and subsequently into neurons (Suter et al., 2009). Based on our results, we find 2D neural induction is easy to perform and is a faster protocol, but it generates less PAX6 positive cells, whilst the 3D neural induction method is longer and requires more labour but generates more PAX6 positive cells.

Several studies have showed that the transcription factor, SOX1, is highly expressed in NPCs (Boissart et al., 2013; Shi et al., 2012a) while SOX9 is expressed in glial progenitors (GPCs) and astrocytes (Pompolo and Harley, 2001; Farmer et al., 2016). In order to analyse differences in neural fate, we studied SOX1 and SOX9 positive cell populations. SOX1 is one of the earliest expressed pan-neuroectodermal transcription factor that appears before PAX6 (Pankratz et al., 2007) and increases when NEPs begin to differentiate towards NPCs, within the embryonic neural tube (Pevny et al., 1998; Li et al., 2009). It is also a marker for proliferating NPCs (Suter et al., 2009; Venere et al., 2012). While SOX9 is expressed in GPCs and is important for its maintenance (Scott et al., 2010), it is also expressed during neural crest stem cell differentiation (Bergsland et al., 2011; Wegner, 2011; Stolt et al., 2003), and this may lead to slightly different progenitor subtypes, such as glial cells. Suter et al., suggested that overexpression of SOX1 in embryoid bodies leads to a large increase in NEP, RG cells and mature neurons (Suter et al., 2009). Based on our quantitative FACS results, we determined the 2D neural induction method generated more SOX1 positive NPCs in the majority of the lines, indicating an early NEP formation compared to the 3D neural induction method, which does suggest a divergence in neural cell fate, however, this could not be verified following neuron differentiation. Furthermore, it has been shown in various

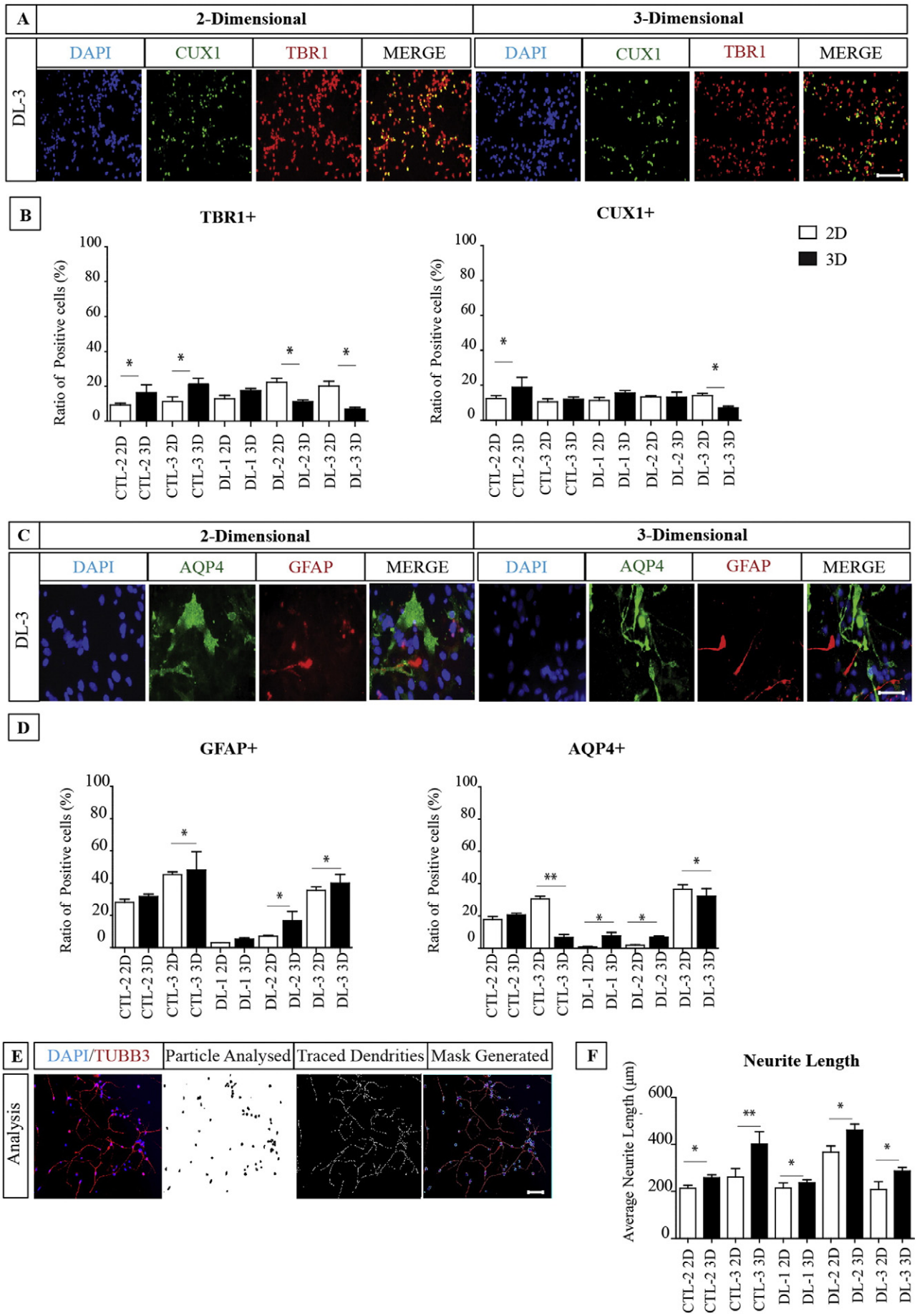
A
2-Dimensional
3-Dimensional
DAPI
CUX1
TBR1
MERGE
DL-3
B
TBR1+
CUX1+
2D
3D
Ratio of Positive cells (%)
CTL-2 2D
CTL-2 3D
CTL-3 2D
CTL-3 3D
DL-1 2D
DL-1 3D
DL-2 2D
DL-2 3D
DL-3 2D
DL-3 3D
C
AQP4
GFAP
D
GFAP+
AQP4+
E
DAPI/TUBB3
Particle Analysed
Traced Dendrities
Mask Generated
Analysis
F
Neurite Length
Average Neurite Length (µm)

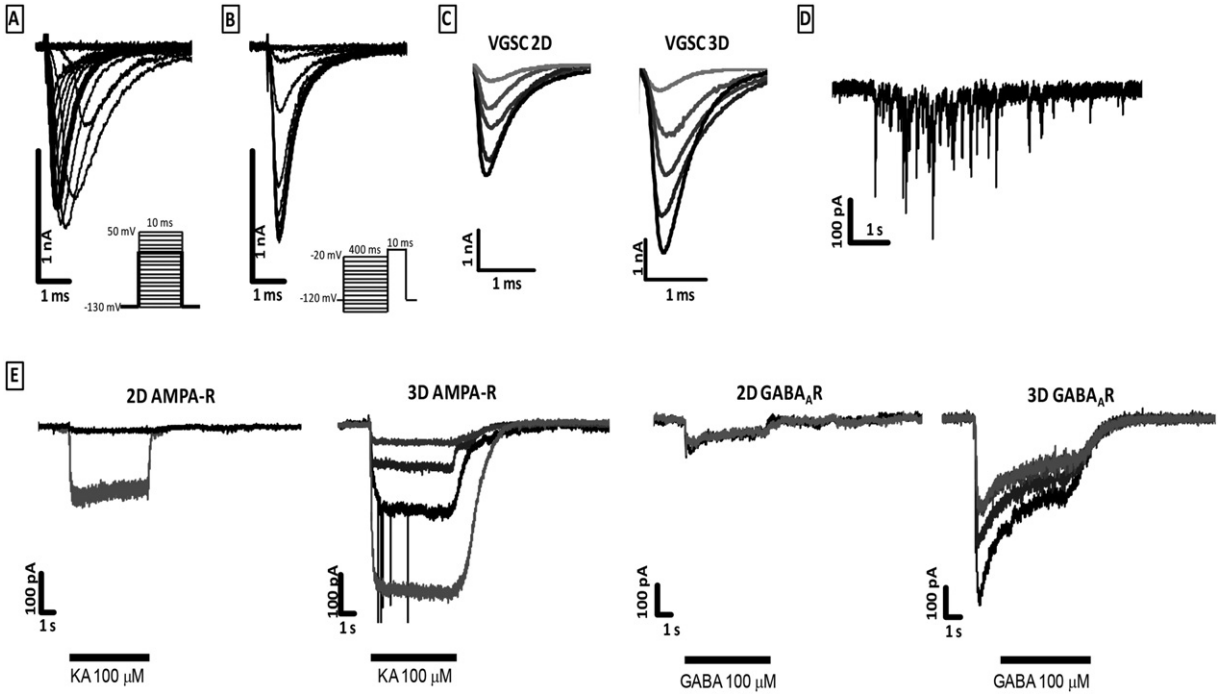

Fig. 7. Ionic currents of neuronal cultures. (A) Example for currents evoked by the activation protocol. Inset shows the voltage pattern. Thick line indicates current evoked by a 10 ms step to 0 mV. (B) Example for currents evoked by the inactivation protocol. (C) Five representative examples for sodium currents from cultures differentiated by the 2D and 3D method. Sodium currents were evoked by depolarizations from −130 to 0 mV. (D) Example for the spontaneous synaptic activity observed in neuronal cultures. (E) Examples for LGIC-mediated currents from cells differentiated by the 2D and 3D methods.

publications, that the upregulation of SOX1 expression results in the promotion of motor neurons (Shimojo et al., 2015), however, this needs to be clarified in future studies.

Numerous hiPSC based studies have reported 3D neuronal differentiation. For example, Kim et al., observed an elevated levels of pathogenic Aβ species in their Matrigel-based 3D culture system compared to the conventional 2D conditions (Kim et al., 2015). It has been shown that 3D culture is critical for sustaining the in vivo ontogeny of neurons (Ribeiro et al., 2012; Blackshaw et al., 1997). Previous studies have shown that 3D differentiation enhances the generation of neurons and neurite outgrowth (Frimat et al., 2015; Sun et al., 2016). In addition, a study by Zhang et al. accelerated neuronal differentiation and maturation of functional neurons from iPSCs in three weeks rather than six weeks in 2D cultures (Zhang et al., 2016a,b). Similar to these studies, our neuritic protrusion analysis demonstrated that neurons cultured with 3D neural induction generated significantly longer neurites, compared to the 2D neural induction. Our neurite length observation is also in agreement with previously described findings (Koh et al., 2008; Kraus et al., 2015; Liu et al., 2016). In our study, we analysed relatively young in vitro cultured neurons, due to technical limitations, which relate to the difficulty in analysing longer projections in older and subsequently denser cultures. It was therefore not possible to measure the neurite length of terminally differentiated mature and electrophysiologically active neurons. Sparsely seeding neurons early in differentiation could be a way to overcome this issue in future studies, since it would be interesting to determine whether neurite outgrowth differences could also be observed at later stages in culture. In addition, we also examined the effects of neural differentiation from hiPSC-derived 2D vs. 3D NPCs towards neurons. Based on the mRNA profiling and ICC, our results also indicated that 3D neural induction showed a modest increase in both MAP2 and TUBB3 in both groups, which is also in accordance with previous findings (Hosseinkhani et al., 2013).

We next sought to determine the proportion of cortical layer identity (TBR1 and CUX1) from these iPSC derived neurons. Our results showed that both conditions resulted in slightly more TBR1 + than CUX1 + cells, which indicates a preference in the generation of the superficial layer IV type cells over the other superficial layers. It is also essential to note that our cultures of iPSC-derived neurons also contain RG, reflecting a heterogeneous environment that is more physiologically relevant to the development of the cells in vivo (Rooney et al., 2016). This has been documented by several other groups in regardless to protocol differences (Johnson et al., 2007; Muratore et al., 2014; Paşca et al., 2015). Our results also showed a line-to-line variability which might be related to the genetic background differences. Taken together, our results demonstrate that there were no intrinsic obstacles for generating different classes of projection neurons from hiPSCs using both neural induction methods; however the 3D method resulted in a higher proportion of NPCs with deep layer neurons that had longer neurites, indicating a slight preference in the 3D method.

Finally, we evaluated the functional characteristics of iPSC-derived neurons. We observed no significant differences between 2D and 3D neural induction methods in their spontaneous activity, or in their LGIC-mediated currents. This suggests that human neurons require longer periods to reach synaptic maturity in in vitro culture conditions, consistent with other observations (Niu et al., 2015). Our study also showed no significant difference between the DL lines vs. the CL lines

Fig. 6. Characterisation of neuronal cultures. (A) Representative immunofluorescent micrographs of DL-3 iPSCs (2D vs. 3D) positive for TBR1/CUX1 (B) Quantification of TBR1/CUX/CULT1 + positive neurons derived from 2D and 3D neural induction. The proportion of cortical layers did not vary between induction methods. (C) Representative immunofluorescent micrographs of CTL-2 iPSCs (2D vs. 3D) positive for GFAP/AQP4 (D) Quantification of AQP4$^+$/GFAP$^+$ astrocytes derived from 2D and 3D NPCs. Results were reported as mean ± SEM of 15 fields from 3 independent cultures (*$p < 0.05$), using Student's *t*-test; by one way ANOVA with a Tukey's post-test (E) Example of workflow of images analysed by Neurite Tracer First: the co-localization, Second: the soma size determined, Third: traced dendrites and Finally: traced and overlaid, Scale bar = 100 μm (F) Bar graphs show neurite outgrowth measurements after 5 days post plating. Neurite measurements show a significant enhancement in neurite length in 3D neural induction method than of 2D. Statistical significance was tested by an unpaired student *t*-test (two tailed). Results were reported as mean ± SEM of 15 fields from 3 independent cultures.

that was similar to Momcilovic et al., where they showed no significant difference in the timeline of neural induction between the patient vs. the control lines (Momcilovic et al., 2016).

5. Conclusion

Somatic cell reprogramming opens the possibility to model human neural development and neurological disorders in a dish, using hiPSCs. Previous 3D neuronal differentiation studies have been performed by embedding NPCs in a scaffold-based system (Choi et al., 2014; Zhang et al., 2016a,b) or by generating organoids (Lancaster and Knoblich, 2014) but they have not directly compared the effects of 2D vs 3D induction on early cell fate, neurite length, differentiation potential, and electrophysiological activities. In this study, we applied an in vitro cellular model to study the neural identity and neural fate of patient-derived and control-derived cells by comparing 2D and 3D neural induction approaches. Based on our results, we were able to document that 3D neuronal induction can promote (i) more PAX6/NESTIN positive NPCs, (ii) young neurons which exhibit longer neurites and (iii) promote glial progenitor formation. Overall, we were able to demonstrate the importance of 3D neural induction across 5 different cell lines.

Author's contribution

AC performed experimental design, implemented the experiments, performed immunocytochemistry, analysed the data and participated in the interpretation of the results and wrote the manuscript. **HXA** designed the experiments, participated in the implementation of experiments, interpretation of the results, reviewed the manuscript and approved the final version. **AO** performed flowcytometry experiments and neural induction experiments. **LNR** was involved in neural induction experiments. **KM** and **LL** performed and analysed electron microscopy data. **TB** performed immunocytochemistry and confocal imaging. **PP** and **AT** was involved in cell culture, **KP** and **AM** performed the electrophysiology measurements and data analysis. **OB** performed karyotyping of the cells. **VH** and **NK** read and revised the paper. **KHK** read and approved the manuscript. **JK** was involved in the experimental design, participated in data analysis, interpretation of the results, and the manuscript preparation. **AD** initiated the study, read and approved the paper. All authors read and approved the final version of the paper.

Conflict of interests

The authors confirm that this paper content has no conflict of interests.

Ethics

Written informed consent had been obtained from the subjects who provided their samples for iPSC derivation. Ethical approvals were obtained from the competent authority to establish and maintain hiPSC lines (ETT-TUKEB 834/PI/09, 8-333/2009-1018EKU).

Supplementary data to this article can be found online at https://doi.org/10.1016/j.scr.2017.10.010.

Acknowledgments

The authors thank C.Nemes, Z.Tancos and E.Varga for providing iPSC cells, I.Block for designing the primers, for M. F. Truszka for preparation of samples for electron microscopy and K.Szczesna for the valuable support. This work was supported by grants from EU FP7 projects (STEMCAM, PIAP-GA-2009-25118; STEMMAD, PIAPP-GA-2012-324451; EpiHealth, HEALTH-2012-F2-278418; EpiHealthNet, PITN-GA-2012-317146) and the Hungarian Brain Research Program (KTIA-NAP-13-2-2014-002) and a national research project RG-IPI-2013_TP7/026.

References

Bergsland, M., Ramsköld, D., Zaouter, C., Klum, S., Sandberg, R., Muhr, J., 2011. Sequentially acting sox transcription factors in neural lineage development. Genes Dev. 25: 2453–2464. https://doi.org/10.1101/gad.176008.111.

Blackshaw, S.E., Arkison, S., Cameron, C., Davies, J.A., 1997. Promotion of regeneration and axon growth following injury in an invertebrate nervous system by the use of three-dimensional collagen gels. Proc. Biol. Sci. 264:657–661. https://doi.org/10.1098/rspb.1997.0093.

Bohl, D., Pochet, R., Mitrecic, D., Nicaise, C., 2016. Modelling and treating amyotrophic lateral sclerosis through induced-pluripotent stem cells technology. Curr. Stem Cell Res. Ther. 11:301–312. https://doi.org/10.2174/1574888X10666150528144303.

Boissart, C., Poulet, A., Georges, P., Darville, H., Julita, E., Delorme, R., Bourgeron, T., Peschanski, M., Benchoua, A., 2013. Differentiation from human pluripotent stem cells of cortical neurons of the superficial layers amenable to psychiatric disease modeling and high-throughput drug screening. Transl. Psychiatr. e294:3. https://doi.org/10.1038/tp.2013.71.

Breunig, J.J., Haydar, T.F., Rakic, P., 2011. Neural stem cells: historical perspective and future prospects. Neuron https://doi.org/10.1016/j.neuron.2011.05.005.

Chambers, S.M., Fasano, C.A., Papapetrou, E.P., Tomishima, M., Sadelain, M., Studer, L., 2009. Highly efficient neural conversion of human ES and iPS cells by dual inhibition of SMAD signaling. Nat. Biotechnol. 27:275–280. https://doi.org/10.1038/nbt.1529.

Chandrasekaran, A., Varga, E., Nemes, C., Táncos, Z., Kobolák, J., Dinnyés, A., 2016. Establishment of induced pluripotent stem cell (iPSC) line from a 63-year old patient with late onset Alzheimer's disease (LOAD). Stem Cell Res. 17:78–80. https://doi.org/10.1016/j.scr.2016.05.014.

Choi, S.H., Kim, Y.H., Hebisch, M., Sliwinski, C., Lee, S., D Avanzo, C., Chen, H., Hooli, B., Asselin, C., Muffat, J., Klee, J.B., Zhang, C., Wainger, B.J., Peitz, M., Kovacs, D.M., Woolf, C.J., Wagner, S.L., Tanzi, R.E., Kim, D.Y., 2014. A three-dimensional human neural cell culture model of Alzheimers disease. Nature 515:274–278. https://doi.org/10.1038/nature13800.

Emdad, L., DSouza, S.L., Kothari, H.P., Qadeer, Z.A., Germano, I.M., 2012. Efficient differentiation of human embryonic and induced pluripotent stem cells into functional astrocytes. Stem Cells Dev. 21:404–410. https://doi.org/10.1089/scd.2010.0560.

Engler, A.J., Sen, S., Sweeney, H.L., Discher, D.E., 2006. Matrix elasticity directs stem cell lineage specification. Cell 126:677–689. https://doi.org/10.1016/j.cell.2006.06.044.

Farmer, W.T., Abrahamsson, T., Chierzi, S., Lui, C., Zaelzer, C., Jones, E.V., Bally, B.P., Chen, G.G., Théroux, J.-F., Peng, J., Bourque, C.W., Charron, F., Ernst, C., Sjöström, P.J., Murai, K.K., 2016. Neurons diversify astrocytes in the adult brain through sonic hedgehog signaling. Science (80-) 351:849–854. https://doi.org/10.1126/science.aab3103.

Frimat, J.-P., Xie, S., Bastiaens, A., Schurink, B., Wolbers, F., den Toonder, J., Luttge, R., 2015. Advances in 3D neuronal cell culture. J. Vac. Sci. Technol. B Nanotechnol. Microelectron. Mater. Process. Meas. Phenom. 33:06F902. https://doi.org/10.1116/1.4931636.

Gaspard, N., Bouschet, T., Herpoel, A., Naeije, G., van den Ameele, J., Vanderhaeghen, P., 2009. Generation of cortical neurons from mouse embryonic stem cells. Nat. Protoc. 4:1454–1463. https://doi.org/10.1038/nprot.2009.157.

Grskovic, M., Javaherian, A., Strulovici, B., Daley, G.Q., 2011. Induced pluripotent stem cells — opportunities for disease modelling and drug discovery. Nat. Rev. Drug Discov. 10: 915–929. https://doi.org/10.1038/nrd3577.

Hadjivassiliou, G., Martinian, L., Squier, W., Blumcke, I., Aronica, E., Sisodiya, S.M., Thom, M., 2010. The application of cortical layer markers in the evaluation of cortical dysplasias in epilepsy. Acta Neuropathol. 120:517–528. https://doi.org/10.1007/s00401-010-0686-x.

Holmqvist, S., Lehtonen, Š., Chumarina, M., Puttonen, K.A., Azevedo, C., Lebedeva, O., Ruponen, M., Oksanen, M., Djelloul, M., Collin, A., Goldwurm, S., Meyer, M., Lagarkova, M., Kiselev, S., Koistinaho, J., Roybon, L., 2016. Creation of a library of induced pluripotent stem cells from Parkinsonian patients. Park. Dis. 2:16009. https://doi.org/10.1038/npjparkd.2016.9.

Hosseinkhani, H., Hiraoka, Y., Li, C.H., Chen, Y.R., Yu, D.S., Hong, P. Da, Ou, K.L., 2013. Engineering three-dimensional collagen-IKVAV matrix to mimic neural microenvironment. ACS Chem. Neurosci. 4:1229–1235. https://doi.org/10.1021/cn400075h.

Hossini, A.M., Megges, M., Prigione, A., Lichtner, B., Toliat, M.R., Wruck, W., Schröter, F., Nuernberg, P., Kroll, H., Makrantonaki, E., Zoubouliss, C.C., Adjaye, J., 2015. Induced pluripotent stem cell-derived neuronal cells from a sporadic Alzheimer's disease donor as a model for investigating AD-associated gene regulatory networks. TL - 16. BMC Genomics 16:84. https://doi.org/10.1186/s12864-015-1262-5.

Jiang, H., Rao, Y., 2005. Axon formation: fate versus growth. Nat. Neurosci. 8:544–546. https://doi.org/10.1038/nn0505-544.

Johnson, M.A., Weick, J.P., Pearce, R.A., Zhang, S.-C., 2007. Functional neural development from human embryonic stem cells: accelerated synaptic activity via astrocyte coculture. J. Neurosci. 27:3069–3077. https://doi.org/10.1523/JNEUROSCI.4562-06.2007.

Kim, Y.H., Choi, S.H., D'Avanzo, C., Hebisch, M., Sliwinski, C., Bylykbashi, E., Washicosky, K.J., Klee, J.B., Brüstle, O., Tanzi, R.E., Kim, D.Y., 2015. A 3D human neural cell culture system for modeling Alzheimer's disease. Nat. Protoc. 10:985–1006. https://doi.org/10.1038/nprot.2015.065.

Koh, H.S., Yong, T., Chan, C.K., Ramakrishna, S., 2008. Enhancement of neurite outgrowth using nano-structured scaffolds coupled with laminin. Biomaterials 29:3574–3582. https://doi.org/10.1016/j.biomaterials.2008.05.014.

Kothapalli, C.R., Kamm, R.D., 2013. 3D matrix microenvironment for targeted differentiation of embryonic stem cells into neural and glial lineages. Biomaterials 34: 5995–6007. https://doi.org/10.1016/j.biomaterials.2013.04.042.

Kraus, D., Boyle, V., Leibig, N., Stark, G., Penna, V., 2015. The neuro-spheroid—a novel 3D in vitro model for peripheral nerve regeneration. J. Neurosci. Methods 246:97–105. https://doi.org/10.1016/j.jneumeth.2015.03.004.

Kriegstein, A., Alvarez-Buylla, A., 2009. The glial nature of embryonic and adult neural stem cells. Annu. Rev. Neurosci. 32:149–184. https://doi.org/10.1146/annurev.neuro.051508.135600.
Lancaster, M.A., Knoblich, J.A., 2014. Generation of cerebral organoids from human pluripotent stem cells. Nat. Protoc. 9:2329–2340. https://doi.org/10.1038/nprot.2014.158.
Li, H., Liu, H., Corrales, C.E., Risner, J.R., Forrester, J., Holt, J.R., Heller, S., Edge, A.S.B., 2009. Differentiation of neurons from neural precursors generated in floating spheres from embryonic stem cells. BMC Neurosci. 10:122. https://doi.org/10.1186/1471-2202-10-122.
Liu, N., Li, Y., Yang, S.T., 2013. Microfibrous carriers for integrated expansion and neural differentiation of embryonic stem cells in suspension bioreactor. Biochem. Eng. J. 75:55–63. https://doi.org/10.1016/j.bej.2013.03.017.
Liu, Y.-Q., Zhan, L.-B., Bi, T.-T., Liang, L.-N., Sun, X.-X., Sui, H., 2016. Neural stem cell neural differentiation in 3D extracellular matrix and endoplasmic reticulum stress microenvironment. RSC Adv. 6:34959–34969. https://doi.org/10.1039/C6RA04370D.
Mariani, J., Vittoria, M., Palejev, D., Tomasini, Livia, Coppola, G., Szekely, A.M., Horvath, T.L., Vaccarino, M.V., 2012. Modeling human cortical development in vitro using induced pluripotent stem cells. Proc. Natl. Acad. Sci. 109:12770–12775. https://doi.org/10.1073/pnas.1202944109/-/DCSupplemental.www.pnas.org/cgi/doi/10.1073/pnas.1202944109.
Molyneaux, B.J., Arlotta, P., Menezes, J.R.L., Macklis, J.D., 2007. Neuronal subtype specification in the cerebral cortex. Nat. Rev. Neurosci. 8:427–437. https://doi.org/10.1038/nrn2151.
Momcilovic, O., Sivapatham, R., Oron, T.R., Meyer, M., Mooney, S., Rao, M.S., Zeng, X., 2016. Derivation, characterization, and neural differentiation of integration-free induced pluripotent stem cell lines from Parkinson's disease patients carrying SNCA, LRRK2, PARK2, and GBA mutations. PLoS One 11:e0154890. https://doi.org/10.1371/journal.pone.0154890.
Muguruma, K., Sasai, Y., 2012. In vitro recapitulation of neural development using embryonic stem cells: from neurogenesis to histogenesis. Develop. Growth Differ. 54: 349–357. https://doi.org/10.1111/j.1440-169X.2012.01329.x.
Muratore, C.R., Srikanth, P., Callahan, D.G., Young-Pearse, T.L., 2014. Comparison and optimization of hiPSC forebrain cortical differentiation protocols. PLoS One 9. https://doi.org/10.1371/journal.pone.0105807.
Nemes, C., Varga, E., Táncos, Z., Bock, I., Francz, B., Kobolák, J., Dinnyés, A., 2016. Establishment of PSEN1 mutant induced pluripotent stem cell (iPSC) line from an Alzheimer's disease (AD) female patient. Stem Cell Res. 17:69–71. https://doi.org/10.1016/j.scr.2016.05.019.
Nestor, M.W., Phillips, A.W., Artimovich, E., Nestor, J.E., Hussman, J.P., Blatt, G.J., 2016. Human inducible pluripotent stem cells and autism Spectrum disorder: emerging technologies. Autism Res. 9:513–535. https://doi.org/10.1002/aur.1570.
Nieto, M., Monuki, E.S., Tang, H., Imitola, J., Haubst, N., Khoury, S.J., Cunningham, J., Gotz, M., Walsh, C.A., 2004. Expression of Cux-1 and Cux-2 in the subventricular zone and upper layers II-IV of the cerebral cortex. J. Comp. Neurol. 479:168–180. https://doi.org/10.1002/cne.20322.
Niu, W., Zang, T., Smith, D.K., Vue, T.Y., Zou, Y., Bachoo, R., Johnson, J.E., Zhang, C.L., 2015. SOX2 reprograms resident astrocytes into neural progenitors in the adult brain. Stem Cell Rep. 4:780–794. https://doi.org/10.1016/j.stemcr.2015.03.006.
Ochalek, A., Nemes, C., Varga, E., Táncos, Z., Kobolák, J., Dinnyés, A., 2016. Establishment of induced pluripotent stem cell (iPSC) line from a 57-year old patient with sporadic Alzheimer's disease. Stem Cell Res. 17:72–74. https://doi.org/10.1016/j.scr.2016.05.020.
Onorati, M., Castiglioni, V., Biasci, D., Cesana, E., Menon, R., Vuono, R., Talpo, F., Goya, R.L., Lyons, P.A., Bulfamante, G.P., Muzio, L., Martino, G., Toselli, M., Farina, C., Barker, R.A., Biella, G., Cattaneo, E., 2014. Molecular and functional definition of the developing human striatum. Nat. Neurosci. 17:1804–1815. https://doi.org/10.1038/nn.3860.
Osumi, N., 2001. The role of Pax6 in brain patterning. Tohoku J. Exp. Med. 193:163–174. https://doi.org/10.1620/tjem.193.163.
Pankratz, M.T., Li, X.-J., LaVaute, T.M., Lyons, E.A., Chen, X., Zhang, S.-C., 2007. Directed neural differentiation of human embryonic stem cells via an obligated primitive anterior stage. Stem Cells 25:1511–1520. https://doi.org/10.1634/stemcells.2006-0707.
Paşca, A.M., Sloan, S.A., Clarke, L.E., Tian, Y., Makinson, C.D., Huber, N., Kim, C.H., Park, J.-Y., O'Rourke, N.A., Nguyen, K.D., Smith, S.J., Huguenard, J.R., Geschwind, D.H., Barres, B.A., Paşca, S.P., 2015. Functional cortical neurons and astrocytes from human pluripotent stem cells in 3D culture. Nat. Methods 12:671–678. https://doi.org/10.1038/nmeth.3415.
Perrier, A.L., Tabar, V., Barberi, T., Rubio, M.E., Bruses, J., Topf, N., Harrison, N.L., Studer, L., 2004. Derivation of midbrain dopamine neurons from human embryonic stem cells. Proc. Natl. Acad. Sci. U. S. A. 101:12543–12548. https://doi.org/10.1073/pnas.0404700101\r0404700101.
Pevny, L.H., Sockanathan, S., Placzek, M., Lovell-Badge, R., 1998. A role for SOX1 in neural determination. Development 125, 1967–1978.
Pompolo, S., Harley, V.R., 2001. Localisation of the SRY-related HMG box protein, SOX9, in rodent brain. Brain Res. 906:143–148. https://doi.org/10.1016/S0006-8993(01)02574-4.
Ribeiro, A., Vargo, S., Powell, E.M., Leach, J.B., 2012. Substrate three-dimensionality induces elemental morphological transformation of sensory neurons on a physiologic timescale. Tissue Eng. A 18:93–102. https://doi.org/10.1089/ten.tea.2011.0221.
Rooney, G.E., Goodwin, A.F., Depeille, P., Sharir, A., Schofield, C.M., Yeh, E., Roose, J.P., Klein, O.D., Rauen, K.A., Weiss, L.A., Ullian, E.M., 2016. Human iPS cell-derived neurons uncover the impact of increased Ras signaling in Costello syndrome. J. Neurosci. 36: 142–152. https://doi.org/10.1523/JNEUROSCI.1547-15.2016.
Roybon, L., Lamas, N., Garcia-Diaz, A., Yang, E., Sattler, R., Jackson-Lewis, V., Kim, Y., Kachel, C.A., Rothstein, J., Przedborski, S., Wichterle, H., Henderson, C., 2013. Human stem cell-derived spinal cord astrocytes with defined mature or reactive phenotypes. Cell Rep. 4:1035–1048. https://doi.org/10.1016/j.celrep.2013.06.021.
Scott, C., Wynn, S., Sesay, A., Cruz, C., Cheung, M., Gaviro, M., Booth, S., Gao, B., Cheah, K., Lovell-Badge, R., Briscoe, J., 2010. SOX9 induces and maintains neural stem cells. Nat. Neurosci. 13:1181–1190. https://doi.org/10.1038/nn.2646.
Shi, Y., Kirwan, P., Livesey, F.J., 2012a. Directed differentiation of human pluripotent stem cells to cerebral cortex neurons and neural networks. Nat. Protoc. 7:1836–1846. https://doi.org/10.1038/nprot.2012.116.
Shi, Y., Kirwan, P., Smith, J., Robinson, H.P.C., Livesey, F.J., 2012b. Human cerebral cortex development from pluripotent stem cells to functional excitatory synapses. Nat. Neurosci. 15 (477–86):S1. https://doi.org/10.1038/nn.3041.
Shimojo, D., Onodera, K., Doi-Torii, Y., Ishihara, Y., Hattori, C., Miwa, Y., Tanaka, S., Okada, R., Ohyama, M., Shoji, M., Nakanishi, A., Doyu, M., Okano, H., Okada, Y., 2015. Rapid, efficient, and simple motor neuron differentiation from human pluripotent stem cells. Mol. Brain 8:79. https://doi.org/10.1186/s13041-015-0172-4.
Stolt, C.C., Lommes, P., Sock, E., Chaboissier, M.C., Schedl, A., Wegner, M., 2003. The Sox9 transcription factor determines glial fate choice in the developing spinal cord. Genes Dev. 17:1677–1689. https://doi.org/10.1101/gad.259003.
Sun, G., Liu, W., Fan, Z., Zhang, D., Han, Y., Xu, L., Qi, J., Zhang, S., Gao, B.T., Bai, X., Li, J., Chai, R., Wang, H., 2016. The three-dimensional culture system with Matrigel and neurotrophic factors preserves the structure and function of spiral ganglion neuron in vitro. Neural Plast. 2016. https://doi.org/10.1155/2016/4280407.
Sun, X.W., Cornwell, X.A., Li, J., Peng, Xs., Joana, O.M., Aalling, Xn., Wang, S., Benraiss, Abdellatif, Lou, N., Goldman, S.A., Nedergaard, Xm, 2017. SOX9 is an astrocyte-specific nuclear marker in the adult brain outside the neurogenic regions. J. Neurosci. 37, 4493–4507.
Suter, D.M., Tirefort, D., Julien, S., Krause, K.-H., 2009. A Sox1 to Pax6 switch drives neuroectoderm to radial glia progression during differentiation of mouse embryonic stem cells. Stem Cells 27:49–58. https://doi.org/10.1634/stemcells.2008-0319.
Takahashi, K., Yamanaka, S., 2006. Induction of pluripotent stem cells from mouse embryonic and adult fibroblast cultures by defined factors. Cell 126:663–676. https://doi.org/10.1016/j.cell.2006.07.024.
Venere, M., Han, Y.-G., Bell, R., Song, J.S., Alvarez-Buylla, A., Blelloch, R., 2012. Sox1 marks an activated neural stem/progenitor cell in the hippocampus. Development 139: 3938–3949. https://doi.org/10.1242/dev.081133.
Tibbitt, M.W., Anseth, K.S., 2012. Dynamic microenvironments: the fourth dimension. Sci. Transl. Med. 4:160ps24. https://doi.org/10.1126/scitranslmed.3004804.
Wattanapanitch, M., Klincumhom, N., Potirat, P., Amornpisutt, R., Lorthongpanich, C., Upratya, Y., Laowtammathron, C., Kheolamai, P., Poungvarin, N., Issaragrisil, S., 2014. Dual small-molecule targeting of SMAD signaling stimulates human induced pluripotent stem cells toward neural lineages. PLoS One 9:e106952. https://doi.org/10.1371/journal.pone.0106952.
Wegner, M., 2011. SOX after SOX: SOXession regulates neurogenesis. Genes Dev. 25: 2423–2428. https://doi.org/10.1101/gad.181487.111.
White, D.L., Mazurkiewicz, J.E., Barrnett, R.J., 1979. A chemical mechanism for tissue staining by osmium tetroxide-ferrocyanide mixtures. J. Histochem. Cytochem. 27: 1084–1091. https://doi.org/10.1177/27.7.89155.
Wilson, P.G., Stice, S.S., 2006. Development and differentiation of neural rosettes derived from human embryonic stem cells. Stem Cell Rev. 2:67–77. https://doi.org/10.1385/SCR:2:1:67.
Yan, Y., Shin, S., Jha, B.S., Liu, Q., Sheng, J., Li, F., Zhan, M., Davis, J., Bharti, K., Zeng, X., Rao, M., Malik, N., Vemuri, M.C., 2013. Efficient and rapid derivation of primitive neural stem cells and generation of brain subtype neurons from human pluripotent stem cells. Stem Cells Transl. Med. 2:862–870. https://doi.org/10.5966/sctm.2013-0080.
Yang, J., Li, S., He, X.-B., Cheng, C., Le, W., 2016. Induced pluripotent stem cells in Alzheimer's disease: applications for disease modeling and cell-replacement therapy. Mol. Neurodegener. 11:39. https://doi.org/10.1186/s13024-016-0106-3.
Yao, S., Chen, S., Clark, J., Hao, E., Beattie, G.M., Hayek, A., Ding, S., 2006. Long-term self-renewal and directed differentiation of human embryonic stem cells in chemically defined conditions. Proc. Natl. Acad. Sci. U. S. A. 103:6907–6912. https://doi.org/10.1073/pnas.0602280103.
Yuan, T., Liao, W., Feng, N.-H., Lou, Y.-L., Niu, X., Zhang, A.-J., Wang, Y., Deng, Z.-F., 2013. Human induced pluripotent stem cell-derived neural stem cells survive, migrate, differentiate, and improve neurological function in a rat model of middle cerebral artery occlusion. Stem Cell Res. Ther. 4:73. https://doi.org/10.1186/scrt224.
Zhang, S.C., Wernig, M., Duncan, I.D., Brüstle, O., Thomson, J. a, 2001. In vitro differentiation of transplantable neural precursors from human embryonic stem cells. Nat. Biotechnol. 19:1129–1133. https://doi.org/10.1038/nbt1201-1129.
Zhang, Y., Sloan, S.A., Clarke, L.E., Caneda, C., Plaza, C.A., Blumenthal, P.D., Vogel, H., Steinberg, G.K., Edwards, M.S.B., Li, G., Duncan, J.A., Cheshier, S.H., Shuer, L.M., Chang, E.F., Grant, G.A., Gephart, M.G.H., Barres, B.A., 2016a. Purification and characterization of progenitor and mature human astrocytes reveals transcriptional and functional differences with mouse. Neuron 89:37–53. https://doi.org/10.1016/j.neuron.2015.11.013.
Zhang, Z., Freitas, B.C., Qian, H., Lux, J., Acab, A., Trujillo, C.A., Herai, R.H., Nguyen Huu, V.A., Wen, J.H., Joshi-Barr, S., Karpiak, J.V., Engler, A.J., Fu, X.-D., Muotri, A.R., Almutairi, A., 2016b. Layered hydrogels accelerate iPSC-derived neuronal maturation and reveal migration defects caused by MeCP2 dysfunction. Proc. Natl. Acad. Sci. 113: 3185–3190. https://doi.org/10.1073/pnas.1521255113.
Zhou, S., Szczesna, K., Ochalek, A., Kobolk, J., Varga, E., Nemes, C., Chandrasekaran, A., Rasmussen, M., Cirera, S., Hyttel, P., Dinnyes, A., Freude, K.K., Avci, H.X., 2016. Neurosphere based differentiation of human IPSC improves astrocyte differentiation. Stem Cells Int. 2016. https://doi.org/10.1155/2016/4937689.